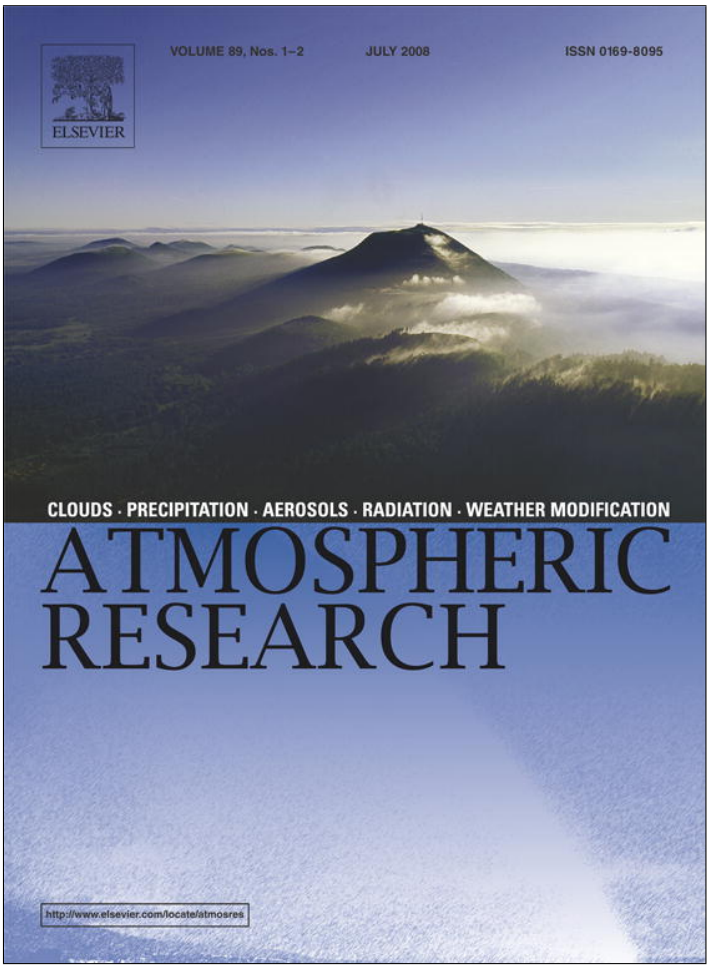

ELSEVIER

Atmospheric Research 89 (2008) 170–180

ATMOSPHERIC RESEARCH

www.elsevier.com/locate/atmos

Indication of water vapor transport into the lower stratosphere above midlatitude convective storms: Meteosat Second Generation satellite observations and radiative transfer model simulations

Martin Setvák [a,*], Daniel T. Lindsey [b], Robert M. Rabin [c], Pao K. Wang [d], Alžbeta Demeterová [a]

[a] *CHMI — Satellite Department, Na Šabatce 17, CZ-14306 Praha 4, Czech Republic*
[b] *NOAA/NESDIS/RAMMB, CIRA/CSU, 1375 Campus Delivery, Ft. Collins, CO 80523, USA*
[c] *NOAA/National Severe Storms Laboratory, 120 David L. Boren Blvd, Norman, OK 73072, USA*
[d] *University of Wisconsin-Madison, 1225 W. Dayton Street, Madison, WI 53706, USA*

Received 16 May 2007; accepted 26 November 2007

Abstract

Past studies using a variety of satellite instruments have demonstrated the possibility of detecting lower stratospheric water vapor against a cold background of deep convective storm tops. The method is based on the brightness temperature difference (BTD) between the water vapor absorption and infrared window bands, assuming a thermal inversion above the cloud top level. This paper confirms the earlier studies, documenting positive BTD values between the 6.2 μm and 10.8 μm bands in Meteosat Second Generation (MSG) Spinning Enhanced Visible and InfraRed Imager (SEVIRI) imagery above tops of deep convective storms over Europe. The observed positive BTD values for a case from 28 June 2005 are compared to calculations from a radiative transfer model, and possible reasons for their existence are discussed. A localized increase in positive BTD is observed at the later stages of storm evolution, and this increase is likely a signal of water vapor being transported by this particular storm from the troposphere into the lower stratosphere.

Keywords: Convective storms; Cloud top microphysics; Stratospheric moisture; Tropopause

1. Introduction

Water vapor (WV) transport from the troposphere to the stratosphere is important not only due to its role as a greenhouse gas (Liou, 1992), but in condensed form it can serve as a surface for a heterogeneous reaction in the destruction of ozone (Solomon, 1999). Recent observations have shown that stratospheric WV has been increasing over at least the last half century (Oltmans et al., 2000; Rosenlof et al., 2001), so understanding its sources and sinks is crucial for climate change studies. It is generally accepted that tropical convection makes a significant contribution to lower stratospheric (LS) WV (Holton et al., 1995), but until recently, few studies have examined the contribution made by convection in the midlatitudes. Fischer et al. (2003) and Hegglin et al.

* Corresponding author. CHMI, Na Šabatce 17, CZ-14306 Praha 4, Czech Republic. Tel.: +420 244033288; fax: +420 244032442.
E-mail address: setvak@chmi.cz (M. Setvák).

0169-8095/$ - see front matter © 2008 Elsevier B.V. All rights reserved.
doi:10.1016/j.atmosres.2007.11.031

(2004) provide independent aircraft measurements of tropospheric-origin air in the lower stratosphere above deep convection in Europe. Dessler and Sherwood (2004) made similar observations near Florida, and they used modeling results to estimate that 40% of summertime extratropical WV on the 340 K potential temperature surface resulted from convection. Wang (2003, 2004, 2007) used a cloud model to show that breaking gravity waves atop a deep convective storm can leave behind WV in the lower stratosphere. None of these studies have shown direct observations of thunderstorms injecting WV into the lower stratosphere.

Many satellite platforms, both polar-orbiting and geostationary, have a channel centered in the water vapor absorption band between 6 and 7 μm. Differencing the brightness temperatures (BT) in this band with those in the infrared (IR) window region (10–11 μm) will generally result in a value below zero, since the WV band's weighting function usually peaks at higher levels, thus at lower temperatures. A band's weighting function indicates the layer from which most of its radiation is emitted, and for the WV band, this is typically in the mid- to upper-troposphere. However, Fritz and Laszlo (1993) noted that positive values occasionally occur over deep convection in the tropics, Ackerman (1996) observed positive values in polar regions, and Schmetz et al. (1997) documented positive values above cold tops of deep convective clouds in both the tropics and mid-latitudes. They reasoned that positive values can only be seen in the presence of a temperature inversion, so that radiation emitted either by a cold ground or opaque storm top is absorbed and re-emitted by overlying water vapor at a *higher* temperature. Such inversions are common at the surface in polar regions and near the tropopause. In the case of deep convective clouds, it is assumed that a warm, widespread water vapor emitting layer is located in the lower stratosphere, just above the storm tops; however, not much is known about its nature and characteristics.

A few alternate mechanisms have been suggested to explain positive BTD values above deep convection, including the non-uniform nature of pixels in conjunction with nonlinearity of the Planck function (Schmetz et al., 1997), possible calibration errors of various satellite sensors, and differing transparency of very thin cirrus between the respective bands (Lattanzio et al., 2005). In their study, Lattanzio et al. (2005) re-examine the questions and answers put forward by Schmetz et al. (1997); the novel element of their study is the rigorous simulation with a radiative transfer model, similar to what is presented in this paper. As the above mentioned studies have shown (by means of quantitative analysis), the WV emission in the lower stratosphere is likely the only mechanism which can explain the observed magnitude of positive BTD above opaque cold cloud tops, though the remaining factors may contribute to the overall BTD to a smaller extent.

This paper uses data from the Spinning Enhanced Visible and InfraRed Imager (SEVIRI) aboard Meteosat Second Generation (MSG), a geostationary satellite centered close to 0° longitude, to document the evolution of WV above convective cloud tops over Europe. Section 2 describes the data and methods; the observations and analysis are found in Section 3; Section 4 shows results from a radiative transfer model used to explain the observations; Section 5 summarizes the paper.

2. Data and processing

The MSG/SEVIRI data used in this study were obtained from the archive of the Czech Hydrometeorological Institute (CHMI); these were received by CHMI's VCS (http://www.vcs.de/spacecom.html) EUMETCast (EUMETSAT Multicast Distribution System, http://www.eumetsat.int/Home/Basic/Common_Content/pdf_td15_eumetcast, EUM TD15) station and archived in VCS Extended Processed Image File Architecture format (XPIF). Selected cases were processed by VCS *2met!* software (http://www.vcs.de/spacecom.html). Visualization was done either by VCS *2met!* software or by the Environment for Visualizing Images (ENVI) software (http://www.ittvis.com/envi/), and the images for this paper were fine-tuned using Adobe Photoshop CS2 (http://www.adobe.com/products/photoshop/). The primary bands used in the analysis were the High Resolution Visible (HRV, SEVIRI band 12), WV6.2 channel (SEVIRI band 5, centered at 6.2 μm), and the IR10.8 window channel (SEVIRI band 9, centered at 10.8 μm), and the difference between the 6.2 μm and 10.8 μm bands (defined here as BTD=BT WV6.2−BT IR10.8), which will be hereafter referred to as the BTD. The reason for using the WV6.2 and not the WV7.3 channel (SEVIRI band 6) are their respective weighting functions. Since the weighting function peak for the WV6.2 band is higher (about 400 hPa for a standard atmosphere at midlatitudes) than that of WV7.3 (about 600 hPa), it can be anticipated that the WV6.2 band will detect moisture above the tropopause (or higher) more efficiently than the WV7.3 would. This anticipation has been sustained to a certain degree by both observations (Section 3) and modeling methods (Section 4). For details on the MSG satellite and its spectral bands, the readers are referred to Schmetz et al. (2002).

3. MSG observations and analysis of storms on 28 June 2005

On 28 June 2005 intense convection formed over northern France, and its evolution was captured with the first MSG satellite, Meteosat-8 (MSG-1). Fig. 1 shows a 10.8 μm image (top) from 1930 UTC and the associated BTD product (bottom). Negative values of BTD are shown in black and white, with the lowest BTD values (10.8 μm BT significantly higher than BT at 6.2 μm) depicted in dark grey to black, and BTD values approaching zero shown in white. Positive BTD values are presented in color according to the color bar inserted in the image (lowest positive BTD values close to zero

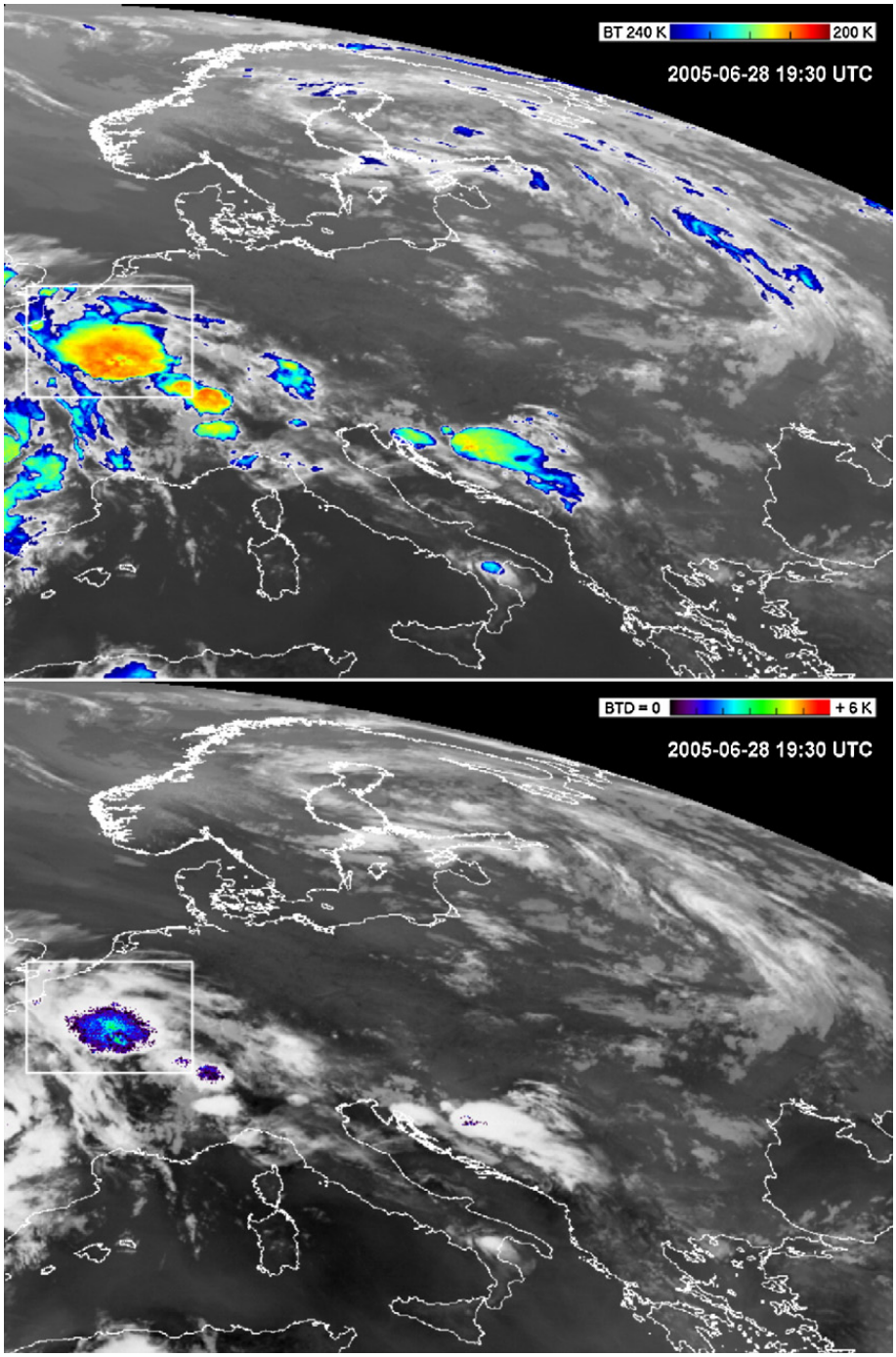

Fig. 1. Meteosat-8 (MSG-1) SEVIRI image from 28 June 2005 at 1930 UTC. Top: IR 10.8 μm band with color enhanced BT range 200–240 K, bottom: BTD (6.2 μm–10.8 μm) product. Grey shades of the BTD product correspond to negative BTD values, while positive values are shown in colors according to BTD colors bar. The white rectangle depicts the region shown in detail on next images. All MSG images of this paper are from CHMI archive. Source of the original MSG data: EUMETSAT.

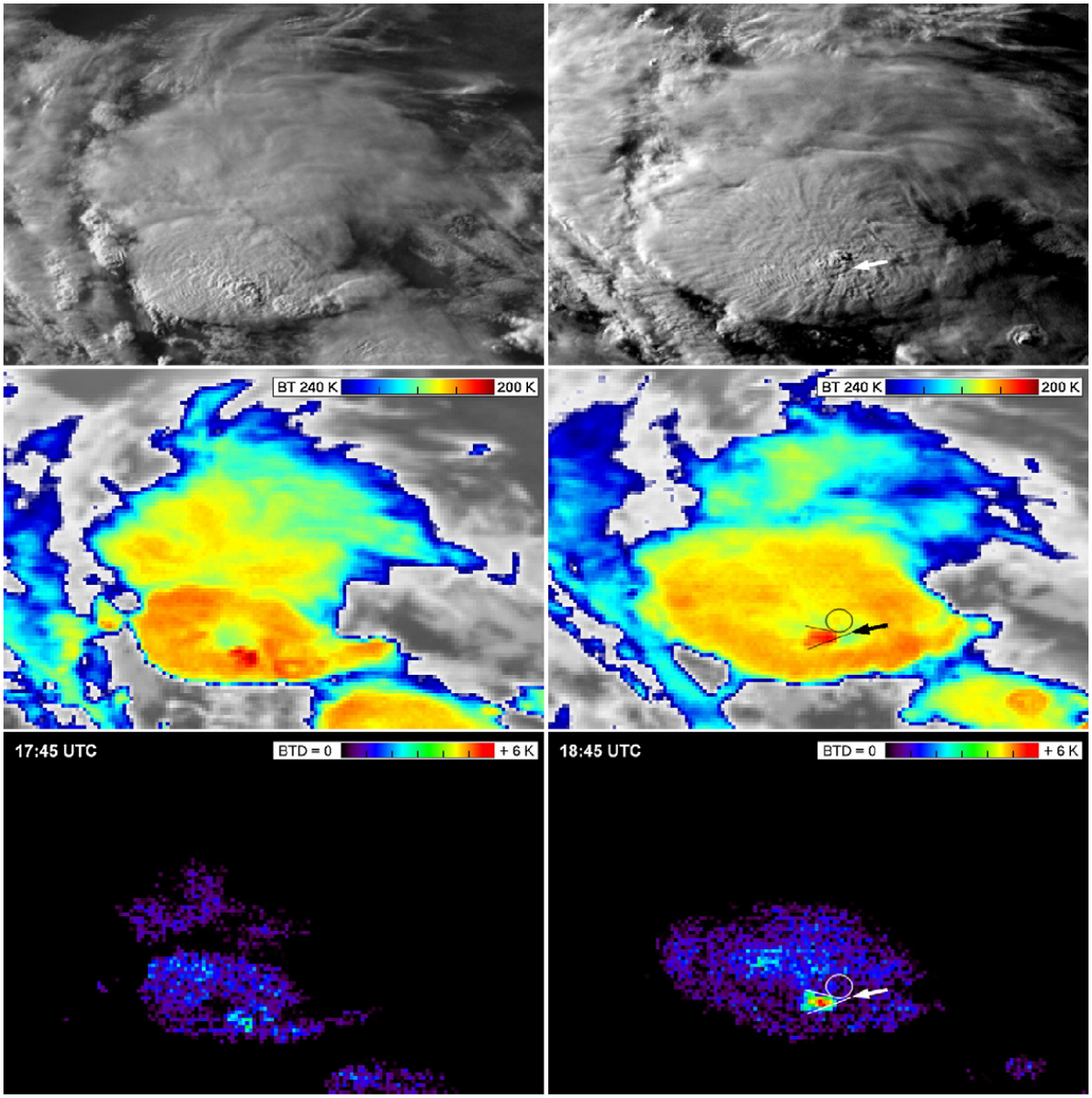

Fig. 2. Details of the storm marked by a rectangle in Fig. 1, at 1745 UTC (left) and 1845 UTC (right). Top — HRV images, middle — color enhanced 10.8 μm images, bottom — color enhanced BTD images, showing positive BTD values only. For discussion of various features outlined in the 1845 image, see the text.

depicted in dark violet to blue, highest BTD values shown in red). As can be seen by comparing the two images, the positive BTD values are found only above the coldest tops of the convective storms over central Europe, approximately within regions whose 10.8 μm BTs are below 210 K. As was discussed by Ackerman et al. (1996), the BTD field is often well correlated (spatially) with the 10.8 μm field itself, with highest positive BTD values found above the coldest IR10.8 spots or areas. This correlation suggests that the radiance at 6.2 μm remains relatively constant above deep convective clouds, so the observed variation in BTD is primarily due to the variation in cloud top temperature seen at 10.8 μm. An example of this correlation (in terms of co-location and magnitude) can be seen in Fig. 2, left column, showing the 28 June 2005 storm at 1745 UTC in SEVIRI HRV band (top), IR10.8 band (middle panel, same enhancement as in Fig. 1), and BTD product (bottom panel, showing positive BTD values only). As will be shown in Section 4, these positive BTD values above the storm are likely a result of WV absorption and re-emission in the lower stratosphere. However, this signal may be due to the presence of a widespread uniform warmer WV layer above the

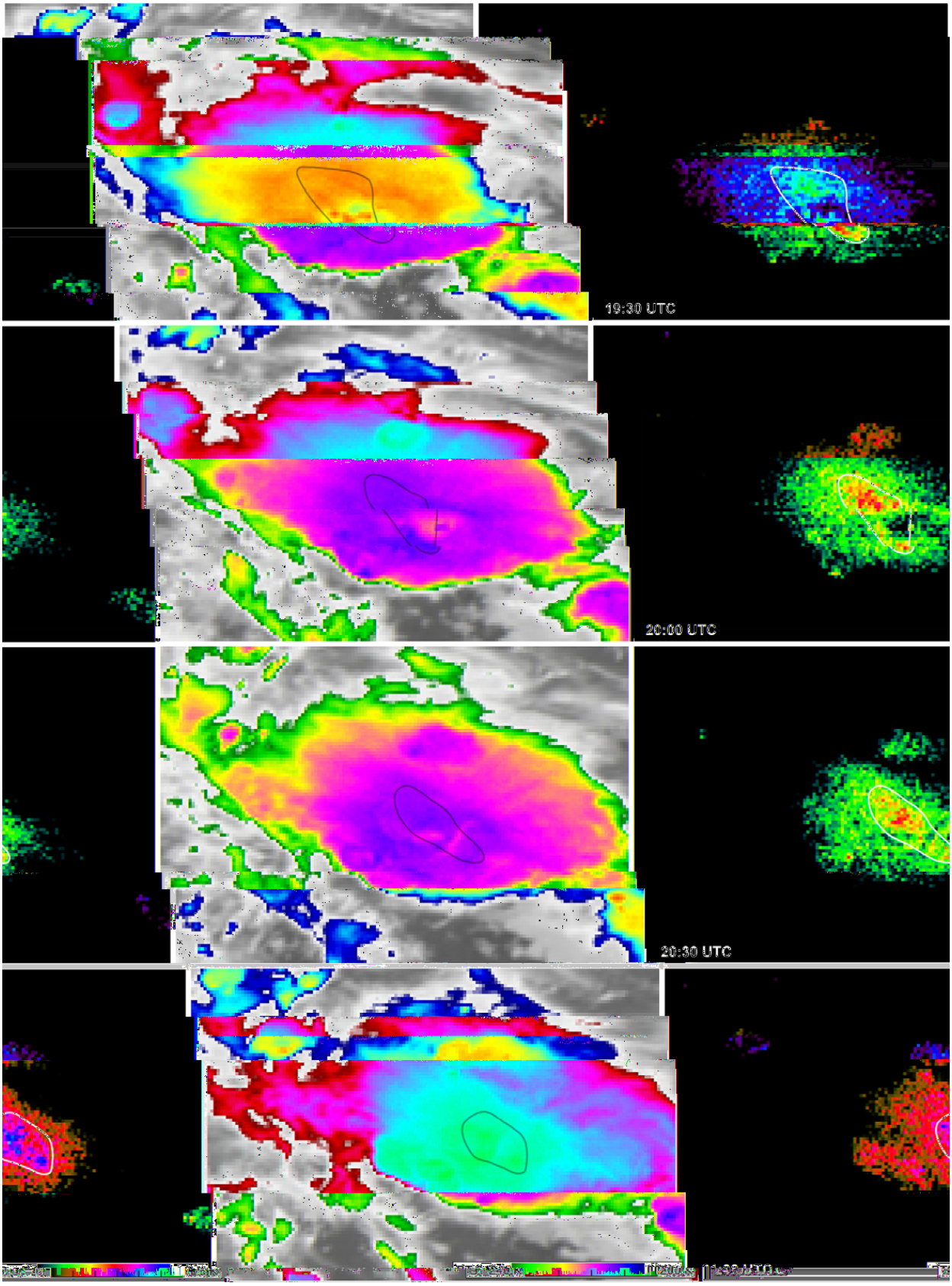

Fig. 3. Evolution of the storm from 1930 to 2100 UTC. Enhanced 10.8 μm images on the left, BTD images right. The area of higher positive values of BTD is outlined in BTD images; this outline is superimposed over the IR 10.8 μm images to show the location of the feature with respect to BT field.

storms (not necessarily related in origin to the storms themselves), rather than locally generated WV above the coldest spots. The thunderstorm tops could simply serve a cold opaque background to make the WV layer become detectable. There are cases where locally increased BTD values seem to be associated with the storm activity; they are the focus of the discussion below.

Setvák et al. (2007) noted that the highest values of BTD may not always be found exactly above the coldest storm tops, and that the spatial characteristics of the BTD and IR window BT fields might be somewhat different. This may indicate local fluctuations of either total amount of lower stratospheric water vapor (LSWV) or its temperature. The largest positive BTD value found on 28 June 2005 occurred at 1845 UTC. Satellite images from 1845 UTC are shown in Fig. 2, right column; the BT at 10.8 μm was 206 K, while the corresponding BTD was +5.7 K. It should be noted that the lowest 10.8 μm BT for the entire life cycle of this storm was found earlier, at 1745 UTC (left column of Fig. 2), when the 10.8 μm BT was 202 K and the corresponding BTD was only 3.4 K. This discrepancy between the 10.8 μm BT and BTD extremes may be explained by two possible mechanisms: 1) A process described by Schmetz et al. (1997) in which an overshooting top penetrates so far into the LSWV layer that the total amount of WV contributing to warm emission in the WV band significantly decreases; or 2) The higher BTD at 1845 UTC may be attributed to a local "vapor source", a mechanism in which water vapor is deposited by the storm itself above its cloud top and quickly balances its temperature with the warmer environment. For the 1745 UTC case, the BT minimum was clearly collocated with a significant overshooting top (as detected in HRV imagery), so both explanations are likely valid. However, at 1845 UTC, the case is less clear. The circle

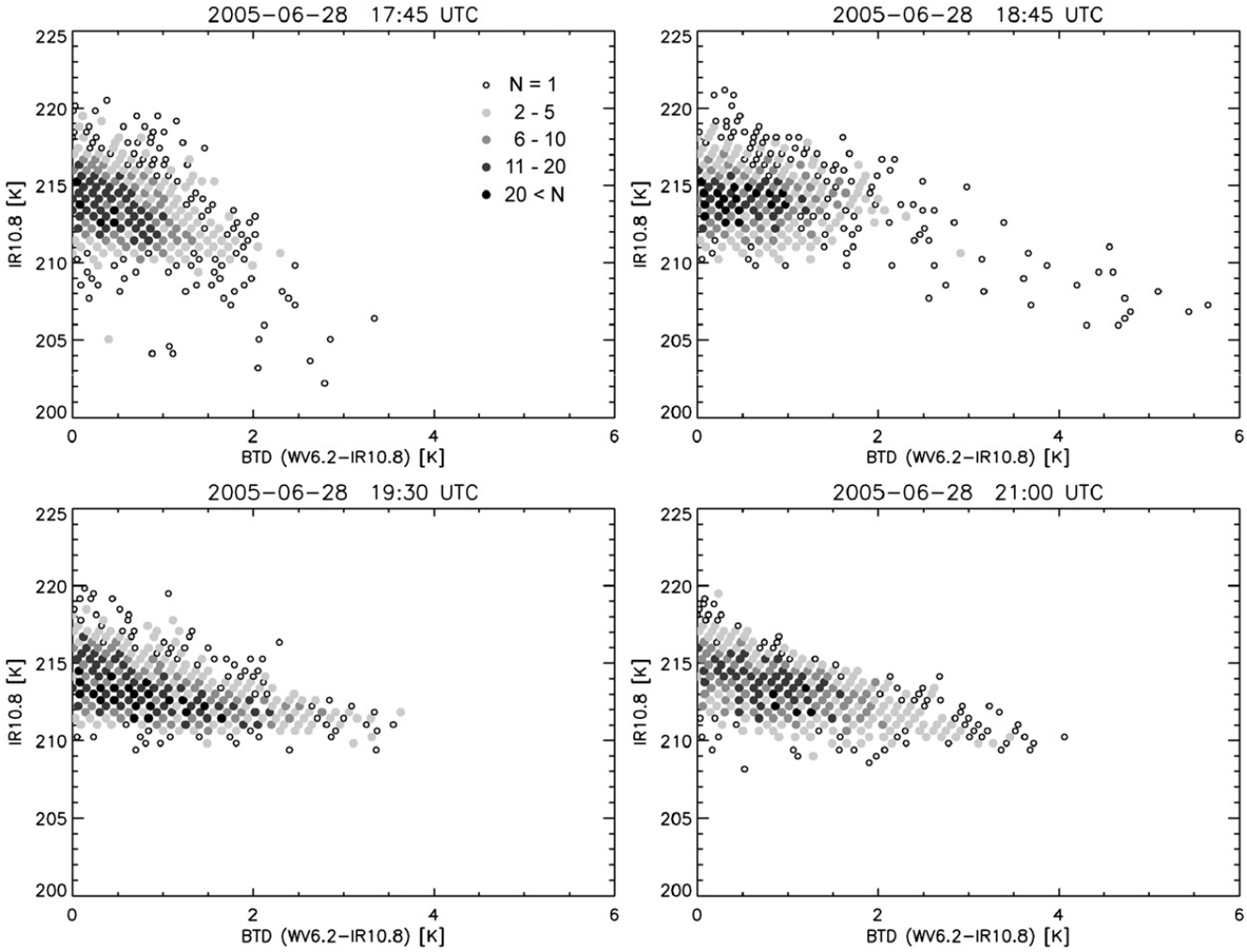

Fig. 4. Scatter plots of BTD (BT 6.2 μm–BT 10.8 μm), horizontal axis, and BT 10.8 μm (range 200–225 K, vertical axis) for the same storm and area as in Figs. 2 and 3, for 1745, 1845, 1930 and 2100 UTC. Only those pixels where the BTD was positive are plotted here; legend for the density distribution (*N*, number of multiple occurrences of the specific value) is shown in the upper left panel.

shown in the 10.8 μm and BTD images at 1845 UTC (right column of Fig. 2) outlines the location of the overshooting top, as determined from the corresponding HRV image. As can be seen, the 10.8 μm BT minimum and BTD maximum are not collocated with the overshooting top; instead, they appear in an area with no obvious vertically elevated or depressed features. Based on shadows and cloud texture evident in the HRV image, it appears that a faint, tiny plume (Levizzani and Setvák, 1996) originates just southeast of the overshooting top area, "streaming" to the west (left, relative to the storm's overshooting dome), just south of the overshooting top. The position of this plume's apparent source is indicated by an arrow, and its outlines from the HRV image are depicted in the corresponding IR10.8 and BTD images at 1845 UTC. Comparing the position and extent of the plume as seen in HRV, it seems that the 10.8 μm BT minimum and BTD maximum are located above the central part of this plume. It is unclear whether the 10.8 μm BT minimum is indeed somehow related to the plume, or just a coincidence.

When using the WV7.3 channel instead of WV6.2 to calculate BTD, the local maximum at 1745 UTC differs by only 0.1 K (+3.3 K using the WV7.2 channel; +3.4 K using WV6.2). At 1845 UTC, however, the BTD maximum is significantly larger using the WV6.2 channel compared to WV7.3: +5.7 K and +3.4 K, respectively. In Section 4, RTM simulations are used to evaluate which channel is most appropriate for computing BTD.

Fig. 3 shows the evolution of the 10.8 μm BT (left column) and the associated BTD (right column). Compared to earlier times (Fig. 2, bottom), the overall trend shows an increase in pixels having BTD greater than +2 K. The area of significant increase is outlined on the BTD images (white lines) and superimposed on the 10.8 μm BT images (black lines) in Fig. 3. This increase may simply be due to a general cooling of the 10.8 μm BT. Scatterplots of BTD and 10.8 μm BT for four times are shown in Fig. 4. Beginning around 1845 UTC, the total number of pixels having BTD greater than +2 K increases. At 1745 UTC, most of the larger positive BTD pixels are associated with very low 10.8 μm BTs, but at 1845, most of these larger BTD pixels have higher 10.8 μm BTs, and this trend continues at 1930 and 2100 UTC. Note in the scatterplots that most of the pixels having BTD greater than +2 K occur for 10.8 μm BTs less than 212 K. We therefore show in Fig. 5 the time evolution of mean BTD for all pixels colder than 212 K, as well as the mean 10.8 μm BT of the same pixels. From the beginning until about 1845 the plot shows some slight variations in both the mean 10.8 μm BT and BTD, but after 1845 these pixels exhibit an increase in mean BTD, accompanied by an increase in mean 10.8 μm BT. Since BTD is defined as the 6.2 μm BT minus the 10.8 μm BT, the mean 6.2 μm BT must have increased more than the mean 10.8 μm BT. The bottom line of this analysis is that WV increased above the coldest cloud tops, and the source of this WV is most likely the storms themselves.

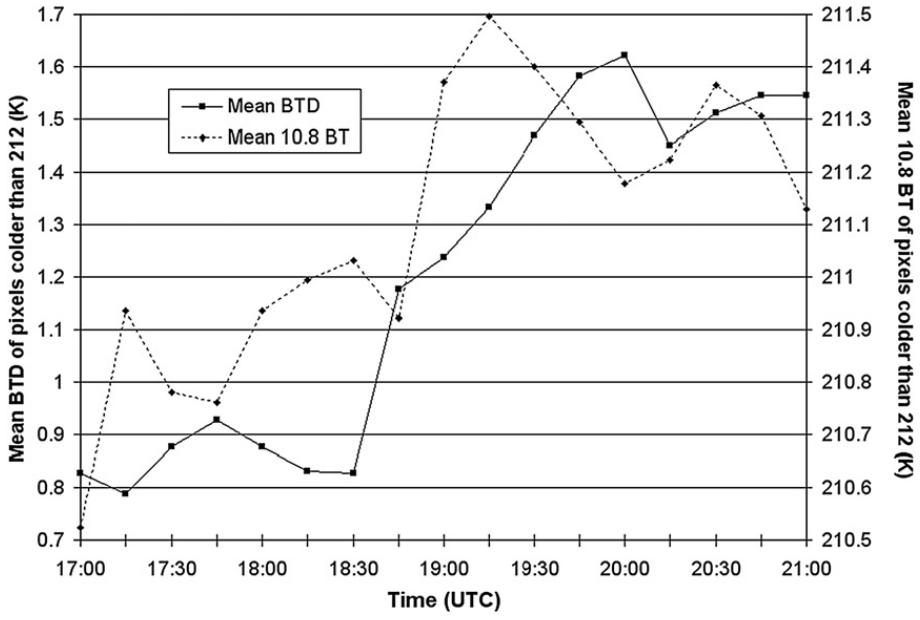

Fig. 5. Time evolution of mean BTD of all pixels having 10.8 μm BT smaller than 212 K for the storm in Figs. 2 and 3 (solid), and mean 10.8 μm BT of the same pixels (dashed).

4. Radiative transfer simulations

The BTD features discussed above could also be explained by cloud top microphysics, i.e. emissivity and transparency effects in combination with temperature gradients at the upper levels of the storms, as well as some other effects (non-uniform nature of pixels in combination with nonlinearity of the Planck function, and possible satellite sensor calibration errors) discussed by Fritz and Laszlo (1993), Ackerman (1996), Schmetz et al. (1997), or Lattanzio et al. (2005). Some of the increased BTD values for the 13 June 2003 storms (Setvák et al., 2007) seem to be located above the semi-transparent portions of the storm's anvil (as indicated by comparison with HRV images), so these could be attributed to transparency effects. However, most of the

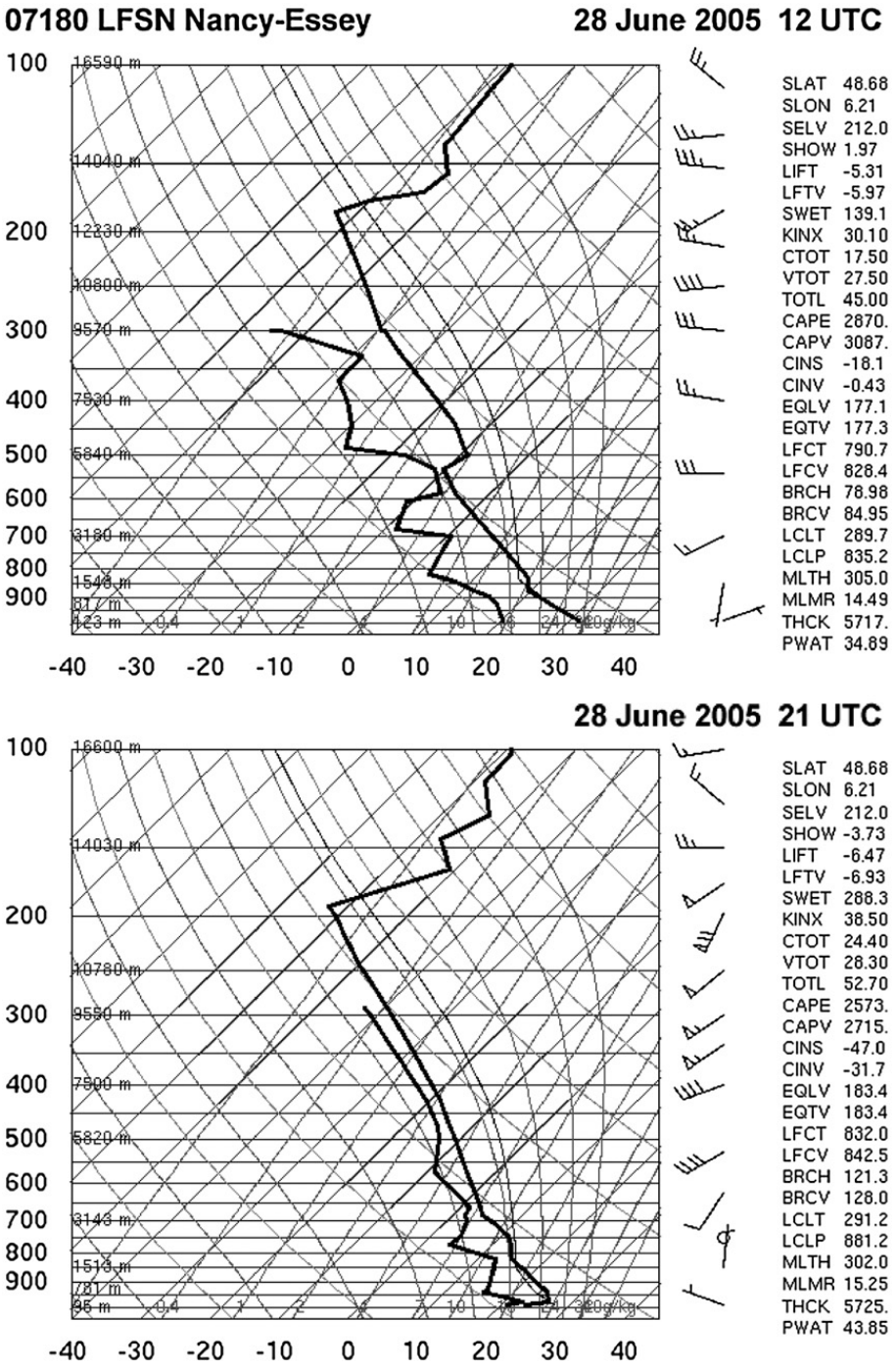

Fig. 6. Soundings from Nancy–Essey at 1200 and 2100 UTC, documenting a strong inversion above 195–190 hPa. Source: University of Wyoming web page.

positive BTD values on 28 June 2005 are located above the core of the storm or close by, so this explanation is unlikely here due to the opaque nature of the cloud.

To achieve some insight on sensitivity of the positive BTD observations to other possible explanations, and to evaluate the necessary amounts of water vapor above the storm top to produce the observed BTD values, a radiative transfer model was used to simulate satellite brightness temperatures. For model details, see Greenwald et al. (2002) and Grasso and Greenwald (2004).

The 12 UTC sounding from Nancy/Essey (Fig. 6, top, about 100 km east of the location of the storm's core at 1845 UTC) was used for the background environmental temperature and WV profiles. Missing dew point data above 300 hPa was obtained from a nearby rawinsonde (Stuttgart, about 250 km east of the storm's core). An ice cloud composed of planar polycrystals (Mitchell 1996) was placed from 10.7–12.7 km, such that its top was located at the observed tropopause. Assuming a Gamma size distribution of the form

$$n(D) = N_0 D^v e^{(-\lambda D)}, \quad (1)$$

where D is the particle diameter, v is the shape parameter (chosen to be 1), and N_0 and λ are constants (Mitchell 2000), ice crystal number concentration and mass mixing ratio were chosen so that the mean crystal diameter was 24 μm and the optical depths at both the water vapor and window infrared bands exceeded 100. As a test, cloud thickness was increased to further increase optical depth, but the resulting brightness temperatures remained approximately the same. This suggests that a 2-km-thick cloud is sufficient to prevent non-negligible transmittance from below. Brightness temperatures at 6.185 μm, 7.34 μm, and 10.7 μm were then computed, and are given in Table 1. These values will serve as the reference case for comparison. Note that the central wavelengths on MSG/SEVIRI are slightly different (6.2 and 10.8); this is a potential source of error, but this error is assumed to be small.

As an initial test, the ice crystal mass mixing ratio and number concentration were adjusted so that the crystal mean diameter was 15 μm and 50 μm (Table 1, rows 2 and 3, respectively). Brightness temperature variation was quite small, suggesting that emissivity effects may be secondary, and other mechanisms are likely responsible for large BTDs. Interestingly, Lattanzio et al. (2005) found that smaller ice crystals increased the BTD, and most of this change (less than 1 K) was due to a change in the infrared band brightness temperatures. Our results show smaller BTD for smaller ice crystals due to more significant changes in the water vapor band brightness temperatures. The reason for these contrasting results is not known. However, in both studies the magnitude of the BTD change is relatively small (less than 1 K).

Table 1
Model calculated satellite brightness temperatures (BT) at three wavelengths, the BT difference (BTD) between bands 6.185 and 10.7, and the BTD between bands 7.34 and 10.7, for 6 tests which are described in the text

Parameter	6.185 BT	7.34 BT	10.7 BT	6.185–10.7	7.34–10.7
Base case	211.04	210.42	210.67	0.37	−0.25
Crystal size 15 μm	210.66	209.89	210.49	0.17	−0.60
Crystal size 50 μm	211.11	210.65	210.46	0.65	0.19
Moist layer 13–14.1 km	211.87	210.59	210.67	1.20	−0.08
Saturated layer 13–14.1 km	212.90	210.88	210.67	2.23	0.21
Overshooting top	208.57	206.08	205.60	2.97	0.48

All units in the table are K.

Next, the environmental WV profile was adjusted by inserting water vapor in the layer from 13.0–14.1 km; this layer begins 300 m above cloud top. Water vapor density values were increased by approximately 0.013 gm^{-3} in the layer, where stratospheric temperatures were near 220 K. This increased the BTD to 1.33, or 0.86 K larger than the reference case (Table 1). Values of BTD greater than 1 K were observed over much of the storm top throughout its lifecycle (Figs. 2 and 3), suggesting that water vapor densities greater than those observed in the environment were present above the cloud top. However, the source of this excess vapor remains uncertain. As an extreme sensitivity test, the layer from 13.0–14.1 km was saturated with respect to liquid water, resulting in a BTD of 2.31 K (Table 1). Lattanzio et al. (2005) found that doubling the stratospheric water vapor content over their reference case produced a BTD increase of 0.91 K, which is approximately the same increase we found in the first test (row 4 of Table 1).

Next, a test was performed to simulate the brightness temperatures associated with an overshooting top. The cloud top height was set to 13.4 km, and assuming a moist adiabatic ascent from the lifted condensation level, its temperature would be approximately 206 K. This matches the observed 10.8 μm brightness temperature at 1845 UTC (Fig. 2). A saturated layer was added from the cloud top to 14.5 km, which represents an extreme moist case. Table 1 shows the model-derived brightness temperatures (under "Overshooting top"). A BTD value near 3 K was less than what was observed

(Fig. 2), but this test shows that inserting a cold overshooting top strengthens the temperature inversion between the cloud top and the lower stratosphere, and therefore increases the BTD. In reality, the actual temperature of the lower stratosphere may have been higher than our pre-storm sounding indicates, in which case the temperature inversion would be even stronger, and the BTD would be greater, perhaps approaching the observed value of 5.7 K. In addition, recent results from the Cirrus Regional Study of Tropical Anvils and Cirrus Layers — Florida Area Cirrus Experiment (CRYSTAL-FACE) indicate that supersaturations with respect to ice may exceed 30% in cold ice clouds (e.g., Jensen and Pfister, 2005). Although we are interested in the layer *above* the cloud layer, if ice supersaturations exceed the values we assume, BTD could be even larger.

Finally, it should be noted that using the WV7.3 channel instead of the WV6.2 channel to calculate BTD resulted in smaller BTD values (Table 1, right column). In particular, for the extreme saturated layer case, the 7.3–10.7 BTD increased by only 0.46 K over the base case, compared to an increase of 1.86 K using the WV6.2 channel. This result shows that the WV6.2 channel is more sensitive to changes in above cloud water vapor, and is therefore is a more appropriate band to use when calculating BTD.

5. Summary and concluding remarks

In this study, cloud top radiative characteristics were studied using MSG SEVIRI imagery over Europe on 28 June 2005. Satellite brightness temperatures at 10.8 μm were subtracted from those in the WV absorption band (6.2 μm), and positive values were observed over very cold cloud tops. It was shown that the positive values were not always correlated with the coldest 10.8 μm pixels, suggesting that the convection served as a local source of LSWV. An increase in the number of pixels having BTD greater than +2 K was observed beginning at 1830 UTC, perhaps in response to multiple overshooting domes transporting WV into the lower stratosphere. In addition to the observational analysis, a radiative transfer model was used to show that an increase in LSWV can lead to positive BTDs, and other possible mechanisms make less significant contributions to the radiative signal.

The case of 28 June 2005 was part of a larger study, within which a total of 13 convective situations above various parts of Europe (each covering several hours or more) were diagnosed using MSG data for the presence of the positive BTD. All of these cases did exhibit some positive BTD for a majority of the diagnosed storms. However, since the BTD was in most cases closely related to BT IR10.8 itself, these were considered a validation of the earlier works of Fritz and Laszlo (1993), Ackerman (1996), Schmetz et al. (1997) and Setvák et al. (2007) only, indicating a more or less uniform warmer moist layer above-storm tops, with no local LSWV generation. Only the 28 June 2005 case showed clear indications of a local LSWV source. This makes the case exceptional and innovative compared to the earlier works mentioned above. Presently, no further studies have been carried out by the authors of this paper for the 2006 and 2007 seasons, but more recent cases documenting positive BTD above cold convective storm tops can be found at the EUMETSAT Image Gallery (http://www.eumetsat.int/Home/Main/Image_Gallery/Satellite_Images_of_the_Month/).

The processes occurring at and above cloud tops of longer-lived or severe storms are still far from well-understood, which makes the BTD interpretation and inferences on LSWV quite difficult and often somewhat speculative. Some processes which may have impacts on the BTD interpretation include modification of the above-storm environment resulting from the storm activity itself (including evaporative cooling of the cloud top or of the layers above) and the gravity wave breaking mechanism (Wang, 2007); both should be considered in future BTD studies.

Although no attempt was made to quantify the amount of WV transported into the stratosphere, this study provided one of the first observations of midlatitude convection serving as an active source of LSWV. Understanding all sources and sinks of the stratospheric WV budget is essential in future climate studies, especially since LSWV has recently been shown to be increasing with time (Oltmans et al., 2000; Rosenlof et al., 2001). In the future, a more rigorous examination of the role played by midlatitude convection in transporting WV into the LS is needed, perhaps by computing the trend in BTD for a large number of mesoscale convective systems. Geostationary satellite imagery is ideal for such an application.

Finally, studies of this kind are likely to be substantiated by utilization of the CALIPSO (Cloud-Aerosol Lidar and Infrared Pathfinder Satellite Observation) satellite and Cloud Profiling Radar of the CloudSat satellite observations, as these will provide quantitatively and qualitatively new information about microphysics, vertical structure of storm tops, and perhaps improve our understanding of the WV budget.

Acknowledgements

Parts of this research were carried out under support of the Grant Agency of the Czech Republic, projects

205/04/0114 and 205/07/0905. PKW wishes to acknowledge the support by US NSF grant ATM-0244505. We also wish to acknowledge Louie Grasso (CIRA) for his support with the RTM simulations.

References

Ackerman, S.A., 1996. Global satellite observations of negative brightness temperature differences between 11 and 6.7 micron. J. Atmos. Sci. 53, 2803–2812.

Dessler, A.E., Sherwood, S.C., 2004. Effect of convection on the summertime extratropical lower stratosphere. J. Geophys. Res. 109, D23301. doi:10.1029/2004JD005209.

Fischer, H., de Reus, M., Traub, M., Williams, J., Lelieveld, J., de Gouw, J., Warneke, C., Schlager, H., Minikin, A., Scheele, R., Siegmund, P., 2003. Deep convective injection of boundary layer air into the lowermost stratosphere at midlatitudes. Atmos. Chem. Phys. 3, 739–745.

Fritz, S., Laszlo, I., 1993. Detection of water vapor in the stratosphere over very high clouds in the tropics. J. Geophys. Res. 98 (D12), 22959–22967.

Grasso, L.D., Greenwald, T.J., 2004. Analysis of 10.7-μm brightness temperatures of a simulated thunderstorm with two-moment microphysics. Mon. Weather Rev. 132, 815–825.

Greenwald, T.J., Hertenstein, R., Vukićević, T., 2002. An all-weather observational operator for radiance data assimilation with mesoscale forecast models. Mon. Weather Rev. 130, 1882–1897.

Hegglin, M.I., Brunner, D., Wernli, H., Schwierz, C., Martius, O., Hoor, P., Fischer, H., Parchatka, U., Spelten, N., Schiller, C., Krebsbach, M., Weers, U., Staehelin, J., Peter, T.h., 2004. Tracing troposphere-to-stratosphere transport above a mid-latitude deep convective system. Atmos. Chem. Phys. 4, 741–756.

Holton, J.R., Haynes, P.H., McIntyre, M.E., Douglass, A.R., Rood, R.B., Pfister, L., 1995. Stratosphere–troposphere exchange. Rev. Geophys. 33, 403–439.

Jensen, E., Pfister, L., 2005. Implications of persistent ice supersaturation in cold cirrus for stratospheric water vapor. Geophys. Res. Lett. 32, L01808. doi:10.1029/2004GL021125.

Lattanzio, A., Watts, P.D., and Govaerts, Y., 2005: Physical interpretation of Warm Water Vapour pixels. EUMETSAT, Technical Memorandum 14. Available from http://www.eumetsat.int/.

Levizzani, V., Setvák, M., 1996. Multispectral, high-resolution satellite observations of plumes on top of convective storms. J. Atmos. Sci. 53, 361–369.

Liou, K.N., 1992: Radia McIntyre, E., Douglass, A.R., Rood, R.B., and Pfister, L., 1995: Radiation and Cloud Processes in the Atmosphere: Theory, Observation, and Modeling. Oxford Univ. Press, New York, 487 pp.

Mitchell, D.L., 1996. Use of mass- and area-dimensional power laws for determining precipitation particle terminal velocities. J. Atmos. Sci. 53, 1710–1723.

Mitchell, D.L., 2000. Parameterization of the Mie extinction and absorption coefficients for water clouds. J. Atmos. Sci. 57, 1311–1326.

Oltmans, S.J., Vömel, H., Hofmann, D.J., Rosenlof, K.H., Kley, D., 2000. The increase in stratospheric water vapor from balloonborne frostpoint hygrometer measurements at Washington, D.C., and Boulder, Colorado. Geophys. Res. Lett. 27, 3453–3456.

Rosenlof, K.H., Oltmans, S.J., Kley, D., Rossell III, J.M., Chiou, E.W., Chu, W.P., Johnson, D.G., Kelly, K.K., Michelsen, H.A., Nedoluha, G.E., Remsberg, E.E., Toon, G.C., McCormick, M.P., 2001. Stratospheric water vapor increases over the past half-century. Geophys. Res. Lett. 28, 1195–1198.

Schmetz, J., Tjemkes, S.A., Gube, M., van de Berg, L., 1997. Monitoring deep convection and convective overshooting with METEOSAT. Adv. Space Res. 19, 433–441.

Schmetz, J., Pili, P., Tjemkes, S., Just, D., Kerkmann, J., Rota, S., Ratier, A., 2002. An introduction to Meteosat Second Generation (MSG). Bull. Am. Meteorol. Soc. 83, 977–992.

Setvák, M., Rabin, R.M., Wang, P.K., 2007. Contribution of the MODIS instrument to observations of deep convective storms and stratospheric moisture detection in GOES and MSG imagery. Atmos. Res. 83, 505–518.

Solomon, S., 1999. Stratospheric ozone depletion: a review of concept and history. Rev. Geophys. 37, 275–316.

Wang, P.K., 2003. Moisture plumes above thunderstorm anvils and their contribution to cross-tropopause transport of water vapor in midlatitudes. J. Geophys. Res. 108 (D6), 5–1–5-15 AAC.

Wang, P.K., 2004. A cloud model interpretation of jumping cirrus above storm top. Geophys. Res. Lett. 31, L18106 10:10.1029/2004GL020787.

Wang, P.K., 2007. The thermodynamic structure atop a penetrating convective thunderstorm. Atmos. Res. 83, 254–262.